Earth Systems and Environment (2024) 8:659–675
https://doi.org/10.1007/s41748-024-00405-0

ORIGINAL ARTICLE

Behavior of Cool and Hot/Warm Air Plumes in Tokyo Revealed by Artificial Intelligence

Ryoichi Doi[1,2]

Received: 7 January 2024 / Revised: 15 March 2024 / Accepted: 6 May 2024 / Published online: 24 July 2024

Abstract

The primary objective of this study was to visualize cool air plumes generated in and coming from urban green areas. Differences in air temperature at meteorological stations at the edges of urban green areas and an urban site in Tokyo in August, November, January, and April were acquired at a time resolution of 10 min for 3 or 6 years. By handling more than 12,800 cases, the automatic neuro-evolution of a deep learning architecture was applied to generalize and visualize the typical wind directions and speeds when cool air plumes were in effect at meteorological stations at the edges of the urban green areas. In some cases, the visualization of cool air plume was successful. For instance, the Tokyo site at the edge of a green area was typically cooler than the urban site in Itabashi when the Tokyo site was subjected to calm wind (<3 m s^{-1}) from the urban green area at night in August. However, in some cases in August, the Tokyo site was hotter than the Itabashi site when the Tokyo site had strong winds from every direction in the daytime, indicating that the strong winds brought heat from heat sources surrounding the urban green area. Thus, the cooling effect at the Tokyo site was at microscale or local scale, while the heating/warming effect was mesoscale. This emphasized that, especially in the daytime in summer, the cool air plumes were prone to be engulfed by greater volumes of hot air plumes from various heat sources. Mechanisms of other related findings are further discussed.

Keywords Cool air plume · Global warming · Artificial intelligence · Deep learning · Urban green area · Urban heat island

1 Introduction

Urban heat islands are seen in most cities in the tropics and even in cooler climate zones in summer (Stewart and Mills 2021). Urban heat islands diminish thermal comfort. Due to the increasing demand for land, cities have spread to include the surrounding green areas. The remaining green areas inside the cities tend to be converted into urban structures such as residential areas and roads. These structures have the capacity to absorb heat converted from solar radiation more than plant canopies. The structures emit the absorbed heat for a period of time, even after sunset (Altan et al. 2019). The cities also have objects that generate and emit heat such as factories, air-conditioners, and offices. Besides the global warming effect of greenhouse gases, cities have various factors that make them hotter than the suburbs and rural areas (Rizwan et al. 2008).

As such, urban green areas are important for cities that are affected by the urban heat island effect. Urban forests and parks are typical urban green areas. The cooling effects of urban green areas have been reported. In Tokyo, land surface temperatures for urban green areas were several degrees (°C) cooler than those of the surrounding urban areas (O'Malley and Kikumoto 2021). Differences in air temperature were also seen between urban and green areas that were within a few hundred meters of each other [e.g., (Kato et al. 2006)]. As in these reports, the cooling intensity of an urban green area is quantitatively expressed as the difference in temperature (ΔT) between the urban site and the green area (Yaşlı et al. 2023).

Previous findings have implied the generation of cool air plumes in urban green areas (Oke 1989). Some review articles have described hot/warm air plumes in association with urban heat island phenomena [e.g., (Mei and Yuan 2022)], and sometimes in association with air pollution (Tzavali et al. 2015). Conversely, a small number of studies on cool

✉ Ryoichi Doi
roird2000@yahoo.com

[1] Faculty of Social-Human Environmentology, Daito Bunka University, 1-9-1 Takashimadaira, Itabashi-ku, Tokyo 175-8571, Japan

[2] Research Center for Tourism, Sustainability and Well-being, University of Algarve, Campus de Gambelas, 8005-139, Faro, Portugal

air plumes in urban green areas have been conducted. If a meteorological station is located near the edge of an urban green area, then, depending on the wind direction at the meteorological station, the effects of cool air plumes and urban heat islands should be detected (Narita et al. 2009). If the wind brings the cool air plume from the green area to the urban side, the meteorological station near the edge of the green area is expected to be cooler than the comparison site in the urban area. In this way, due to the effect of cool air plumes, significant ΔT values were expected in the Tokyo region.

The Tokyo and Nerima meteorological stations run by the Japan Meteorological Agency are located at the edges of green areas (Fig. 1). In addition, in Tokyo, there is an urban meteorological station, namely the meteorological station of Itabashi City Hall, which is surrounded by busy offices and other urban structures. In this study, ΔT values were obtained by subtracting air temperature values at the Tokyo or Nerima site from those at the Itabashi site. The greatest ΔT values were thought to be associated with the appearance of cool air plumes in the green areas. The primary objective of this study was to visualize the appearance of cool air plumes by identifying the trends in wind directions and speed at the sites at the edges of the green areas (Fig. 2).

Precise observations have been made previously to describe the mechanisms of the cooling effects of green areas [e.g., (Narita et al. 2004; Sugawara et al. 2021)]. These previous studies had the advantage of precision. Measurements were made within a few days or within a week because of the labor intensity needed, which was difficult to continue for a longer time. These measurements would be meaningful if the observed cooling effects as ΔT values and other meteorological results were typical and thus could be extrapolated to a large number of cases acquired over a longer period of study. Mid-term to long-term datasets improved the accuracy and precision of the prediction of meteorological outcomes, such as electrical power generation relying on wind (Moschella et al. 2019). To identify the typical conditions that appear with cool air plumes, this study used values from meteorological variables acquired every 10 min in August, November, January, and April, and for multiple years at the Itabashi site and in the green areas to calculate the ΔT values.

Another requirement for the reliable identification of the trends in wind direction and speed when cool air plumes appear at the edges of the green areas is that the observed greatest ΔT values themselves should be truly typical in terms of cool air plume appearance. The typical meteorological conditions when the greatest ΔT values are seen may be

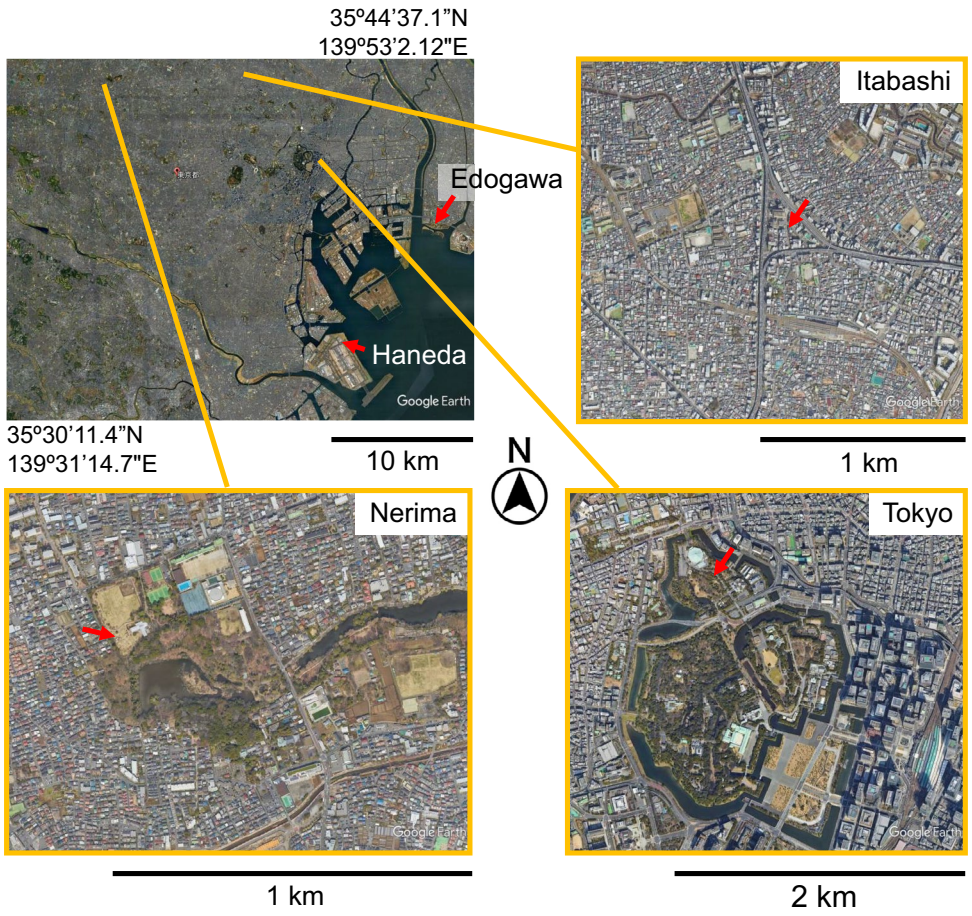

Fig. 1 Locations of the meteorological stations. The red arrows indicate the locations

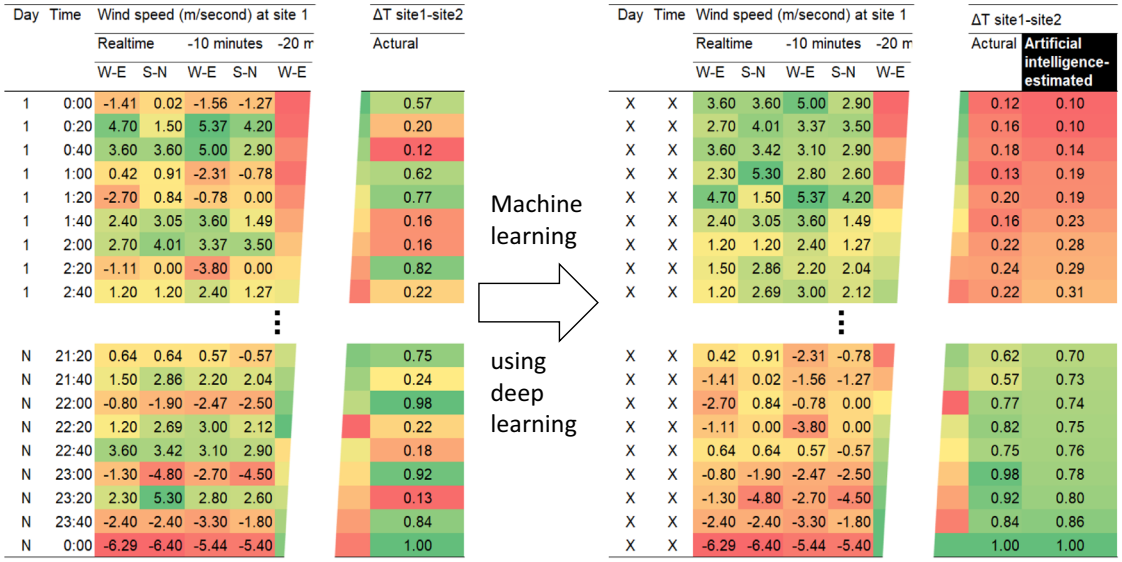

Fig. 2 Identification of wind directions and speeds at the time points of greatest and smallest ΔT values. W–E and S–N indicate west–east and south–north wind vector components, respectively

described by meteorological variables other than wind direction and speed, as in the case of deposition of air pollutants predicted by meteorological variables (Afrin et al. 2021). Even though wind direction and speed were expected to be the most significant determinants of ΔT, there may be more meteorological variables that are significant determinants of ΔT. To enhance the reliability of ΔT prediction based on the empirical approach explained later, in addition to wind direction and speed, more meteorological variables were involved in maximizing the reliability of ΔT prediction and thus identification of the wind direction and speed when the greatest ΔT values occurred.

For these reasons, values for several meteorological variables at many time points (cases) were acquired for the reliable identification of the trends in wind direction and speed when cool air plumes appeared. To enable the reliable identification of the wind trend, artificial intelligence methods are realistic options because of their size and multivariate data structure (Skubalska-Rafajłowicz 2014). According to a recent review article, the involvement of artificial intelligence in urban green space studies is the most recent development (Farkas et al. 2023). A small number of studies has applied artificial intelligence approaches in relation to urban green areas. For example, Oukawa et al. (2022) applied an artificial intelligence method, namely, random forest, to the mapping of urban heat islands and green spaces in Londrina, Brazil (Oukawa et al. 2022).

Machine learning is an artificial intelligence method. Among machine learning methods, deep learning was selected as a method for the analysis of the datasets in this study (Pichler and Hartig 2023). Deep learning mimics the structure and function of the human brain. Deep learning often classifies discretely different objectives, such as cohorts. Also, the deep learning architectures can estimate values for individual cases on continuous measures if the squared error function is used as the loss function, which maximizes the accuracy and precision of the estimation (Doi 2019). Furthermore, the deep learning architectures are automatically optimized to achieve the best estimation of values to be determined. Automatic running for the optimization is referred to as neuro-evolution, which was adopted in this study when using the deep learning architecture. Eventually, the neuro-evolution processes resulted in optimized deep artificial neural network architectures (Doi 2021).

Therefore, this study was conducted to visualize cool air plumes at the meteorological stations on the edges of green areas in Tokyo. Visualization was made by depicting the trend in wind direction and speed at the time points when the greatest ΔT values were estimated. This study is the first to visualize the movement of cool air plumes to the meteorological stations from the nearby tree canopies by analyzing datasets acquired at a precise time resolution of 10 min in four seasons in multiple years. However, depending on conditions, the meteorological stations in the green areas were found to be hotter than the urban site. The cooling and heating mechanisms are discussed.

2 Methods

2.1 Site Description

According to Köppen (Köppen 1931), the current study area (Fig. 1) belongs to the humid subtropical zone (Cfa). Tokyo

meteorological station is located in Kitano-maru Park, Chiyoda-ku, Tokyo, Japan (35° 41′ 30.4″ N, 139° 45′ 4.8″ E; Fig. 1). The park borders the Imperial Palace, which has a large green area of 115 ha (Akihito et al. 2016). Itabashi City Hall is in Itabashi-ku, Tokyo (35° 45′ 4.8″ N, 139° 42′ 32.8″ E). The meteorological station is located on the rooftop of the city hall. Nerima meteorological station is in a park in Nerima-ku, Tokyo (35° 44′ 21.1″ N, 139° 35′ 35.5″ E). Edogawa and Haneda meteorological stations are located in Kasai Rinkai Park (35° 38′ 19.9″ N, 139° 51′ 49.1″ E) and Haneda International Airport (35° 33′ 51.3″ N, 139° 47′ 22.1″ E), respectively. The altitudes are 51 m (Nerima) above sea level or lower.

2.2 Meteorological Data

For the Tokyo, Nerima, Edogawa, and Haneda sites, the meteorological data were retrieved from the Japan Meteorological Agency web page (https://www.jma.go.jp/jma/indexe.html). At the meteorological measurement sites, air temperature, wind speed, wind gust, wind direction, and precipitation were recorded every 10 min. Also, a period of solar radiation within 10 min was available for the Tokyo, Nerima, and Edogawa sites. Meteorological data from the Itabashi site were retrieved from the city hall's weather web page (http://itabashi.tenki.ne.jp/itabashi/iwsb/000_index.php?pnt=001&t=1678709856447). For the Itabashi site, air temperature, wind speed, wind gust, wind direction, and precipitation were available at intervals of 10 min.

This study used the 10 min-resolution data for August in 2017, 2018, 2019, 2020, 2021, and 2022 (6 years) as well as the data for January, April, and November in 2018, 2019, and 2020 (3 years) in analyzing differences in air temperature between Itabashi and Tokyo or Nerima. In the region, August, November, January, and April are the months that represent summer, autumn, winter, and spring, respectively. Some wind speed values were not numerically available but were given as "calm" instead. The "calm" data were regarded as and converted to nil (0).

The difference in air temperature between the two sites (ΔT) was determined using the following equation:

$$\Delta T_{site1-site2}(^{\circ}C) = \text{air temperature at site 1 } (^{\circ}C) - \text{air temperature at site 2 } (^{\circ}C) \quad (1)$$

Wind speed/gust and direction were combined and converted to west–east and south–north vector components using the following equations:

$$\text{West - east wind vector component} = \text{wind speed } (ms^{-1}) \times \sin(\theta) \quad (2)$$

$$\text{South - north wind vector component} = \text{wind speed } (ms^{-1}) \times \cos(\theta) \quad (3)$$

where θ is wind direction. θ is 0° when the wind direction is north, 90° when east, 180° when south, and 270° when west. There were 16 θ values. Western and southern winds were positive, and eastern and northern winds were negative.

2.3 Machine Learning

Each ΔT and other meteorological variables were linearly 0 to 1 re-scaled to enable machine learning. The following computation processes were made using Sony Neural Network Console version 2.7 (Sony, Tokyo, Japan). For each meteorological variable, in addition to the value at time 0 (real time), values at 10, 20, 30, 40, 50, and 60 min before time 0 were also used. The converted values derived from the August data on $\Delta T_{Itabashi\text{-}Tokyo}$ (hereafter, $\Delta T_{ITB\text{-}TKY}$) were first used to identify the best artificial intelligence architecture in terms of predictability of $\Delta T_{ITB\text{-}TKY}$.

To identify the best artificial intelligence architecture, the neuro-evolution of a deep learning architecture described by Doi (2019) was applied. The independent meteorological variables from the Itabashi site were wind speed (west–east and south–north vector components), wind gust (west–east and south–north vector components), and precipitation. Thus, there were five independent meteorological variables. As each of these meteorological variables had values recorded every 10 min from 0 (real time) to 60 min before, the Itabashi dataset consisted of 35 independent variables. Likewise, the Tokyo dataset consisted of 42 independent variables because the meteorological variables included period of solar radiation within 10 min in addition to those recorded at the Itabashi site. Eventually, 77 independent variables were involved instead of the 83 variables in the previous report (Doi 2019). One-half of the data was used as the training dataset, and the other half as the validation dataset. The training dataset consisted of values at the 10th, 30th, and 50th minutes of every hour. The other values at the 20th, 40th, and 60th minutes of every hour were used to prepare the validation dataset. Thus, the time resolution became 20 min for the training and validation datasets. A randomly assigned 75% (training)—25% (validation) dataset was also prepared from the August $\Delta T_{ITB\text{-}TKY}$ dataset to compare with the 50–50% dataset.

First, using neuro-evolution, the August $\Delta T_{ITB\text{-}TKY}$ dataset was analyzed. More than 500 architectures were automatically examined at an epoch number of 500. The architecture depicted in Fig. 3 was determined as the best architecture in terms of predictability of $\Delta T_{ITB\text{-}TKY}$. The best architecture was used as the starter architecture for the analysis of

other datasets applying further neuro-evolution to identify the ad hoc optimized architecture for each ΔT dataset, as described later. The 0–1 re-scaled values for the 77 independent variables were taken in by the input layer. The next layer referred to as the Affine layer hands over 1568 values derived from the 77 values to the next activation layer, called the exponential linear unit layer. This activation layer handles input values greater than 0 as they are, and hands them over to the next batch normalization. This layer, meanwhile, converts input values less than 0 to values between 0 and − 1.67 according to the mathematical function, then transfers them to the following batch normalization layer. The batch normalization layer normalizes the output values for the multiple batches. This stabilizes the subsequent processes. In this study, a batch size of 512 was adopted. There were three other activation layers, namely, the leaky rectified linear unit layer, the scaled exponential linear unit layer, and the sigmoid layer. The leaky rectified linear unit and scaled exponential linear unit layers have similar functions to the exponential linear unit layer, but the shapes of output–input lines are somewhat different. The sigmoid layer converts the values given by the previous process. The output values fell between 0 and 1. Finally, the squared error function determines the value for the case by minimizing the total error in the regression of actual and estimated values. The optimizer was the Adam algorithm at alpha = 0.001, beta 1 = 0.9, beta 2 = 0.999, and epsilon = 10^{-8}.

Some data were missing although this was rare. These cases were removed. The six cases for the following 60 min were also removed. Eventually, the total numbers of cases were 26,691 (August, Itabashi–Tokyo), 12,819 (November, Itabashi–Tokyo), 13,390 (January, Itabashi–Tokyo), 12,931 (April, Itabashi–Tokyo), 26,783 (August, Itabashi–Nerima), and 13,368 (January, Itabashi–Nerima). Temperature and wind direction/speed data obtained in August at the Edogawa and Haneda sites were added to the August $\Delta T_{ITB\text{-}TKY}$ analysis to evaluate the additive effects for the $\Delta T_{ITB\text{-}TKY}$ estimation. In this analysis, the number of cases decreased to 26,650 due to missing values for the Edogawa or the Haneda site.

By neuro-evolution starting from the starter architecture (Fig. 3), 20 more architectures were generated. Minor changes in architecture were automatically made to optimize the ΔT estimation. Among the generated 20 architectures, the best architecture was selected in terms of ΔT predictability. Among the validation data, the cases of the smallest or greatest 200 ΔT values were estimated. Then, the wind directions and speeds at the 200 time points for the smallest or greatest 200 ΔT were identified, as depicted in Fig. 2.

Fig. 3 The starter architecture for neuro-evolution to identify the ad hoc optimized architecture for ΔT estimation. Abbreviations, ELU, exponential linear unit; LeakyReLU, leaky rectified linear unit; SELU, scaled exponential linear unit

2.4 Statistical Analyses

XLStat version 2021.4.1 (Addinsoft Inc., Paris, France) was used for statistical analysis.

2.5 Normalized Difference Vegetation Index

QGIS 3.22.8 was used to obtain values of the normalized difference vegetation index (Rouse et al. 1974) for 30 × 30 m-resolution pixels in the Landsat 8 imagery acquired at 10:15 AM Tokyo time on 6 August 2015. The Landsat dataset was a geometrically corrected level 1 product. The determination was made relying on the following equation:

$$\text{Normalized difference vegetation index} = \frac{\text{Near infrared} - \text{red}}{\text{Near infrared} + \text{red}} \quad (4)$$

Where red and near-infrared are reflectance measurements for red (640–670 nm wavelength, band 4) and near-infrared (850–880 nm wavelength, band 5), respectively. The normalized difference vegetation index indicates gradients between extremely urbanized and vegetation-rich areas. The richer the vegetation, the closer the value converges to 1.

2.6 Tokyo Demographic Data

A 2020 demographic dataset was retrieved from the Japanese government site (https://www.e-stat.go.jp/).

2.7 Measurements of Land and Water Surface Temperature

In the park at the Nerima site, land and water surface temperatures were measured using a thermography camera F30W (Nippon Avionics Co. Ltd., Yokohama, Japan) between 4:11 AM and 4:16 AM on 27 July 2023. The Nerima meteorological station has a lawn slope around it. The land surface temperatures at the western slope were measured. The park has a pond (Fig. 1). The water surface temperatures were measured.

3 Results

3.1 Climatic Variations in Tokyo and Machine Learning of the Datasets

In the current study area in Fig. 1, spatiotemporal variations of meteorological variables were perceivable (Fig. 4, Table 1). For example, at the Nerima site in August, wind speed and gust tended to be smaller than those at the other sites, while precipitation was richer. The Edogawa and Haneda sites had strong winds due to their seaside locations. In January, the Nerima site tended to have cooler nights than the Tokyo and Itabashi sites.

In the current study area in Fig. 1, warm and humid southern winds are dominant in summer (Fig. 5). The dominance results in greater precipitation than in January (Table 1). Meanwhile, in winter, the prevailing dry winds come from the northwestern directions. In Tokyo, April and November are spring and autumn, respectively. These months are intermediate in terms of air temperature. November was the sunniest month and April was the windiest month.

The results of the analysis of variance for ΔT are summarized in Table 2. Year, month, time slot, and the difference between Itabashi and Tokyo/Nerima were the significant sources ($p < 0.001$). All interactions were significant at $p = 0.001$. The linear model described 20.8% of the entire variation. Machine learning of the datasets and estimation of ΔT values resulted in Fig. 6, in which the R^2 values were between 0.525 (November, Itabashi–Tokyo) and 0.742 (January, Itabashi–Nerima). The slope varied from 0.516 (November, Itabashi–Tokyo) to 0.754 (January, Itabashi–Nerima). The high significance ($p < 0.001$) of the ΔT estimation by the involved variables showed that the wind directions and speeds that resulted in the smallest/greatest 200 ΔT values would be reliably identified. When wind speed and gust data alone were used, the R^2 values decreased, for example, 0.554 to 0.426 (August, Itabashi–Tokyo), from 0.540 to 0.380 (August, Itabashi–Nerima), from 0.587 to 0.497 (January,

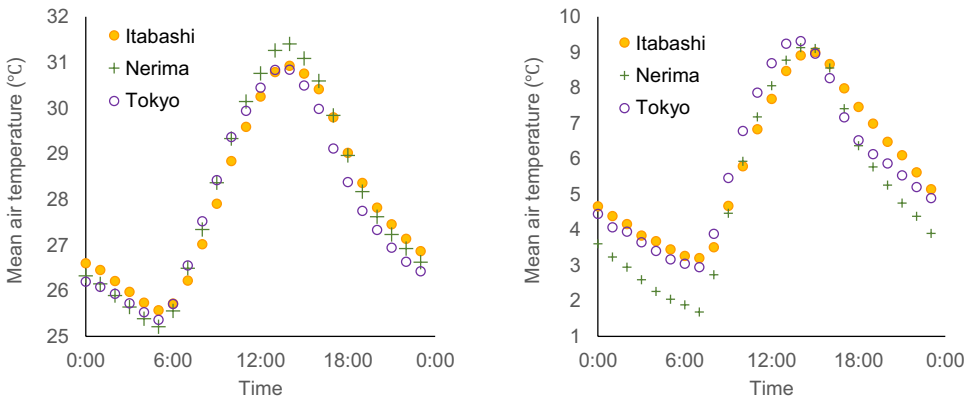

Fig. 4 Mean hourly temperatures at the Itabashi, Nerima, and Tokyo sites in August (left) and January (right)

Table 1 Descriptive statistics for the meteorological variables used in this study

Month and year	Site	Air temperature (℃)			Wind speed (m s^{-1})			Wind gust (m s^{-1})			Precipitation (mm/10 min)			Solar radiation (min/10 min)		
		Min	Max	Mean	Min	Max	Mean	Min	Max	Mean	Min	Max	Mean	Min	Max	Mean
January	Itabashi	−3.00	18.6	5.84	0.00	10.5	2.34	0.00	23.7	5.48	0.00	2.50	0.01	Not available		
2018–2020	Tokyo	−3.90	18.0	5.78	0.00	9.70	2.62	0.00	21.5	5.09	0.00	2.00	0.01	0.00	10.0	2.35
	Nerima	−6.60	18.7	5.10	0.00	7.90	1.76	0.00	15.7	3.85	0.00	1.50	0.01	0.00	10.0	2.24
April	Itabashi	2.90	29.2	14.4	0.00	12.4	2.84	0.00	31.8	7.01	0.00	3.50	0.03	Not available		
2018–2020	Tokyo	2.30	28.3	14.5	0.10	12.6	3.31	0.40	23.2	6.32	0.00	6.50	0.04	0.00	10.0	2.84
August	Itabashi	18.0	37.0	28.0	0.00	10.7	2.67	0.30	26.8	6.41	0.00	14.5	0.03	Not available		
2017–2022	Tokyo	18.4	36.9	27.8	0.10	12.0	3.06	0.50	22.2	5.60	0.00	16.0	0.03	0.00	10.0	2.35
	Nerima	18.3	38.9	28.0	0.00	11.8	1.21	0.00	25.1	3.46	0.00	37.5	0.04	0.00	10.0	2.24
	Edogawa	18.8	35.8	27.5	0.00	17.9	4.54	Not used			Not used			Not used		
	Haneda	19.2	36.7	28.0	0.00	18.2	5.38	Not used			Not used			Not available		
November	Itabashi	2.40	24.4	13.8	0.00	7.90	1.92	0.00	21.0	4.67	0.00	3.50	0.02	Not available		
2018–2020	Tokyo	1.90	24.8	13.7	0.20	8.90	2.38	0.60	16.9	4.54	0.00	4.50	0.02	0.00	10.0	5.03

Itabashi–Tokyo), and from 0.742 to 0.673 (January, Itabashi–Nerima). These changes indicated that the 56 wind variables alone accounted for a large part of the variations of ΔT and that the 21 meteorological variables other than the 56 wind variables assisted the predictability. The estimation of August $\Delta T_{ITB\text{-}TKY}$ using the 75% (training) − 25% (validation) dataset resulted in negligible improvement of R^2 value from 0.554 (Fig. 6) to 0.556.

3.2 Wind Directions and Speeds at the Time Points of the Estimated Smallest or Greatest 200 ΔT Values

The most typical wind directions and speeds were constant within 60 min at the time points when the smallest/greatest 200 ΔT values were estimated (Fig. 7). Wind directions and speeds at the time points indicated the spatiotemporal changes described below.

3.2.1 August, Itabashi–Tokyo

In August, an obvious wind direction tendency was seen when the largest 200 $\Delta T_{ITB\text{-}TKY}$ values were estimated; thus Itabashi was typically hotter than Tokyo (Fig. 6). The most typical wind directions at the Tokyo site were south to southeast (Fig. 7a). The wind was relatively calm. At the 200 time points, a similar trend of wind direction was confirmed at the Itabashi site. Among the 200 cases, no cases had wind speeds of 3 m s^{-1} or greater at the Tokyo site, indicating slow but stable movement of the cool air plumes to the meteorological station. This relationship in which the Tokyo site was typically cooler was observed mainly at night (Table 3).

There were some cases in which the Itabashi site was cooler than the Tokyo site (Fig. 6). The smallest 200 $\Delta T_{ITB\text{-}TKY}$ values were estimated when the Tokyo site was subjected to strong winds from almost all directions while the Itabashi site did not have southeastern, southern, and southwestern wind (Fig. 7a). The timeslot was mainly 8.00 to 16.00 (Table 3). A significant number of heat sources, such as offices and roads, were recognized around the Imperial Palace and the Tokyo site (Fig. 1). These urban areas with small values of normalized difference vegetation index had few green areas (Fig. 8), which had more heat sources than those with greater values of normalized difference vegetation index.

3.2.2 November, Itabashi–Tokyo

In November, the trend of wind direction and speed had common features and these were different from those in the August data. When the largest 200 $\Delta T_{ITB\text{-}TKY}$ values were estimated at the Tokyo site, at 0 time (real time), six cases had wind speeds that exceeded 3 m s^{-1}. However,

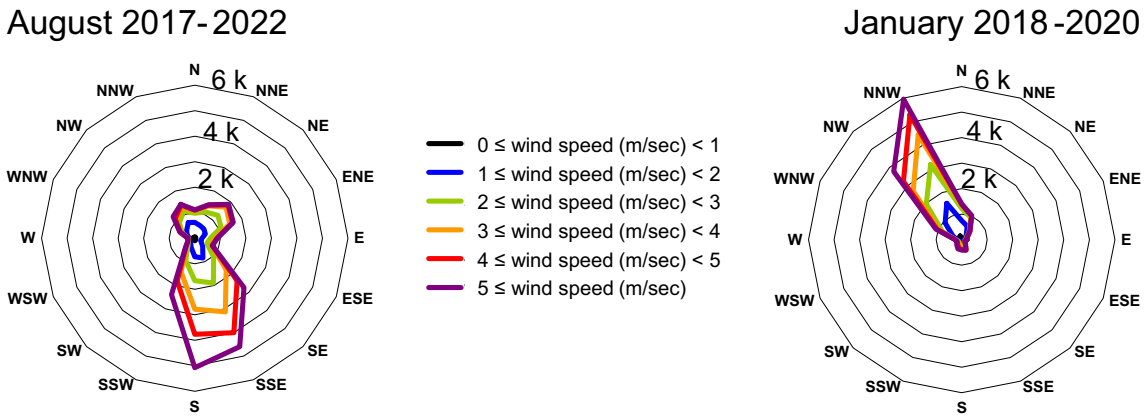

Fig. 5 Wind roses for the periods of August 2017–2022 and January 2018–2020 based on the Tokyo data at a resolution of 10 min

Table 2 Summary of analysis of variance of difference in air temperature between two sites (ΔT)

Source of variance	Type III sum of squares	Degrees of freedom	Mean square	*F*	Significance (*p* value)
Corrected model	22,497	95	237	256	< 0.001
Intercept	573	1	573	619	< 0.001
Year	853	5	171	184	< 0.001
Month	2199	3	733	792	< 0.001
Time slot	8961	5	1792	1936	< 0.001
Itabashi–Tokyo or Itabashi–Nerima (Site)	554	1	554	599	< 0.001
Year × Month	264	6	44	48	< 0.001
Year × Time slot	400	25	16	17	< 0.001
Year × Site	286	2	143	154	< 0.001
Month × Time slot	1102	5	220	238	< 0.001
Month × Site	3169	1	3169	3424	< 0.001
Year × Month × Time slot	319	10	32	34	< 0.001
Year × Month × Site	43	2	21	23	< 0.001
Year × Time slot × Site	65	10	7	7	< 0.001
Month × Time slot × Site	94	5	19	20	< 0.001
Year × Month × Site × Time slot	120	10	12	13	< 0.001
Error	85,729	92,617	1		
Corrected total	110,622	92,713			

*Corrected $R^2 = 0.208$

when the smallest 200 $\Delta T_{ITB\text{-}TKY}$ values were estimated, the northwestern wind was more dominant at the sites than in August, indicating that the season was heading to winter (Table 1, Fig. 5). As shown in Table 3, 131 among the greatest 200 $\Delta T_{ITB\text{-}TKY}$ values were estimated between 16.00 and 20.00, which is earlier than August. In contrast, the smallest 200 $\Delta T_{ITB\text{-}TKY}$ values were indicated to occur mainly between 8.00 and 16.00.

3.2.3 January, Itabashi–Tokyo

In January, the greatest 200 $\Delta T_{ITB\text{-}TKY}$ values were estimated when the Itabashi site had weak southeastern, southwestern, and western winds, while the Tokyo site had gentle winds from similar directions, except that southern winds were more frequent than the Itabashi site (Fig. 7c), suggesting that the Itabashi City Hall received warm air from the significant urban heat sources (Figs. 8 and 9). Approximately one-half (101) of the greatest 200 $\Delta T_{ITB\text{-}TKY}$ occurred within a time slot between 16.00 and 20.00 (Table 3). Conversely, when the smallest 200 $\Delta T_{ITB\text{-}TKY}$ values were estimated,

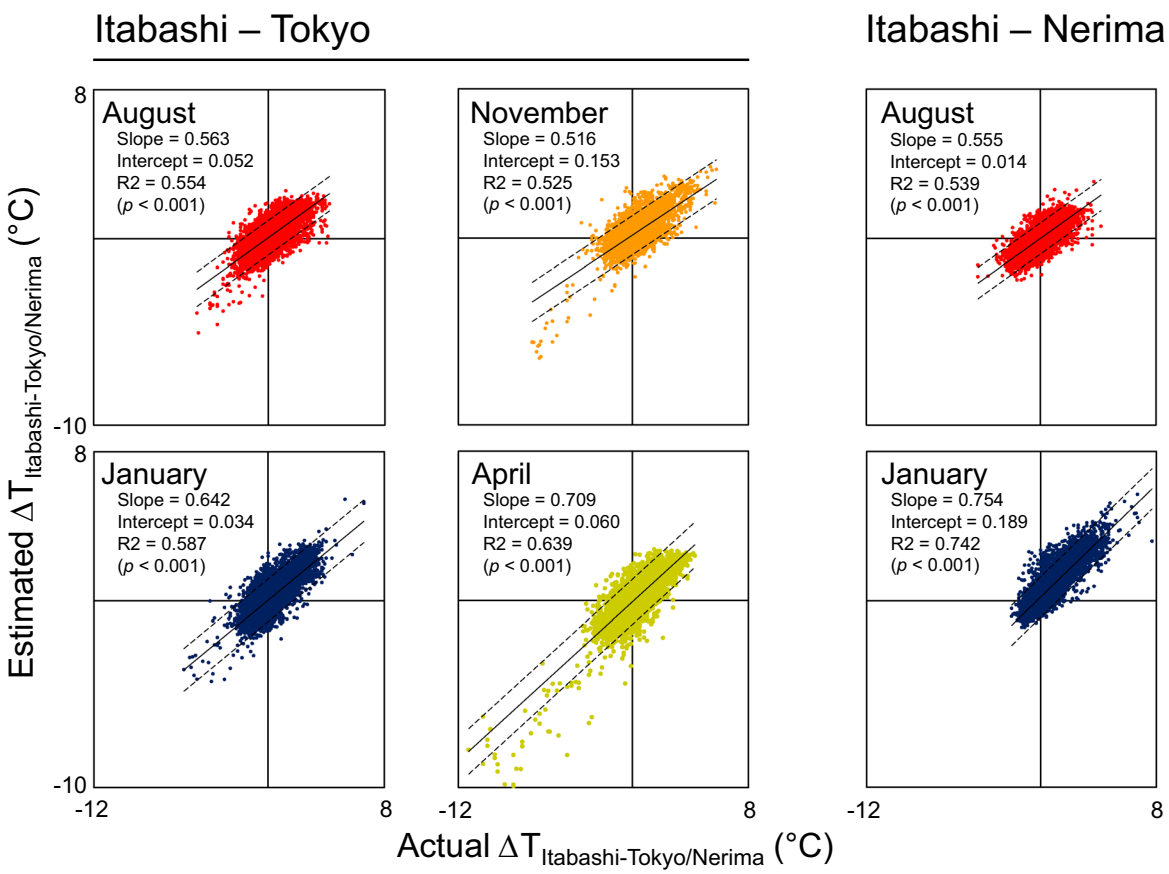

Fig. 6 Correlations between actual and estimated ΔT using the ad hoc optimized artificial intelligence architecture. The dashed lines indicate 95% prediction intervals

the trends of wind direction and speed were quite different from those in August. Both the Itabashi and Tokyo sites had strong winds mainly from the northwest.

3.2.4 April, Itabashi–Tokyo

Figure 7d has similarities to the August plots (Fig. 7a), possibly because of the period leading into summer (Table 1). When the greatest 200 $\Delta T_{ITB\text{-}TKY}$ values were estimated, as in August, the Tokyo site tended to have calm winds, although three cases out of 200 had wind speeds greater than 3 m s^{-1}. The greatest 200 $\Delta T_{ITB\text{-}TKY}$ values occurred mainly at night, as shown in Table 3. Table 3 also shows that the time slot patterns for the greatest and smallest $\Delta T_{ITB\text{-}TKY}$ values were very similar to those of the August data, again indicating the proximity to summer weather conditions.

3.2.5 August, Itabashi–Nerima

When the greatest 200 $\Delta T_{Itabashi–Nerima}$ (hereafter, $\Delta T_{ITB\text{-}NRM}$) in August were estimated, mainly at night (Table 4), the wind direction and speed patterns did not clearly differ from those when the smallest 200 $\Delta T_{ITB\text{-}NRM}$ values were (Fig. 7e). Although southeastern winds from the park aside the Nerima site were expected to cool the meteorological station, the frequency of southeastern winds was very low. At the Nerima site in August, the frequency of southeastern winds, once expected to cool the site, was very significantly smaller (687/24536) than that of southern winds (4581/24536) (Chi-square statistic 3225, $p < 0.00001$).

3.2.6 January, Itabashi–Nerima

In January, the greatest 200 $\Delta T_{ITB\text{-}NRM}$ values were estimated, typically for the cases between 20.00 and 8.00 (Table 4), when the Itabashi site had western winds while the Nerima site had extremely calm winds (Fig. 7f). Meanwhile, the smallest 200 $\Delta T_{ITB\text{-}NRM}$ values were estimated when the entire study area in Fig. 1 was dominated by strong northwest winds, typically between 8.00 and 16.00.

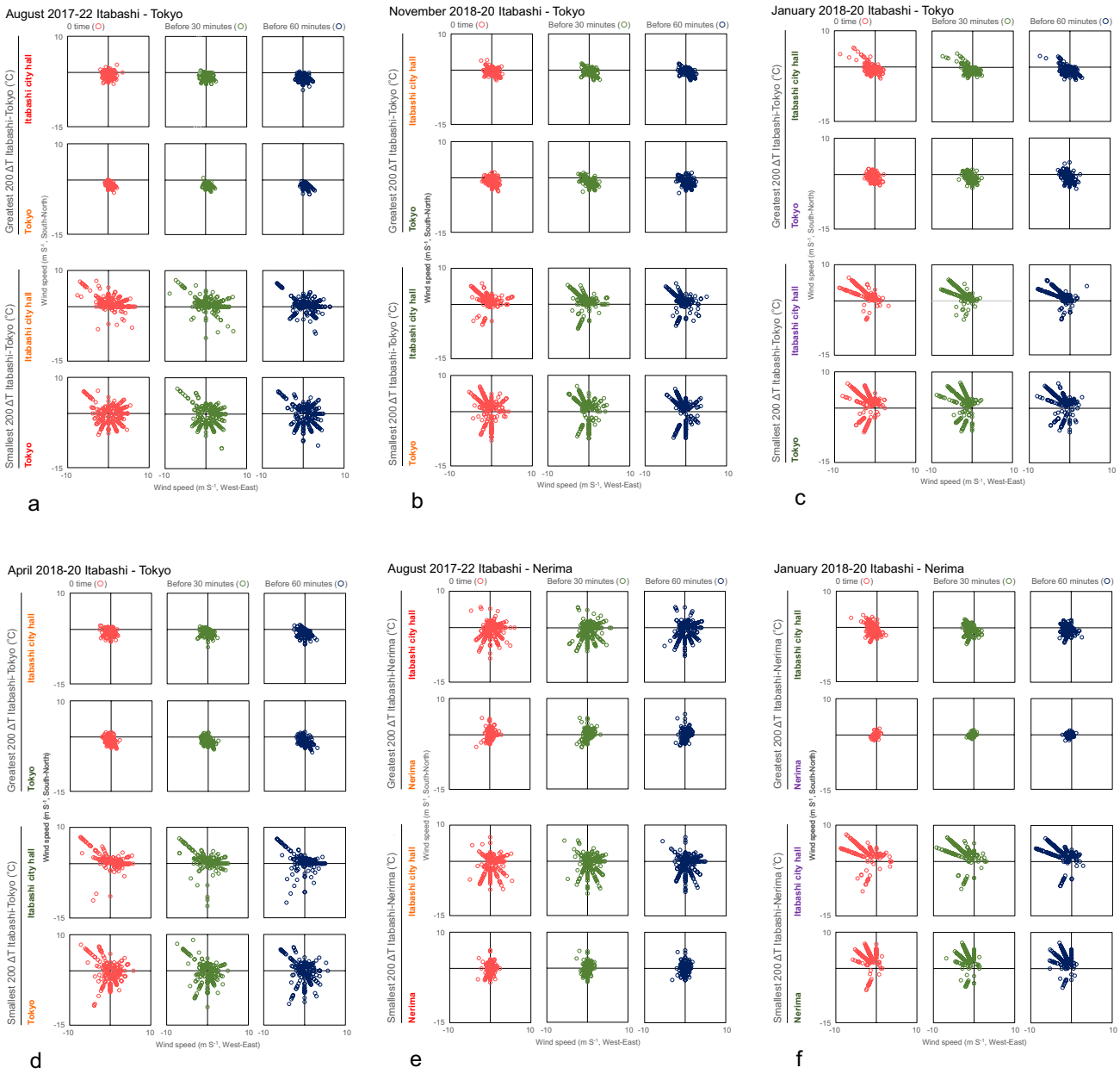

Fig. 7 Wind directions and speeds for the cases of the estimated smallest or greatest 200 ΔT values

Table 3 Time slots for the cases of the estimated smallest/greatest 200 $\Delta T_{Itabashi–Tokyo}$ values

Time slot	August 2017-2022			November 2018-2020			January 2018-2020			April 2018-2020		
	Total cases	Greatest 200 △T	Smallest 200 △T	Total cases	Greatest 200 △T	Smallest 200 △T	Total cases	Greatest 200 △T	Smallest 200 △T	Total cases	Greatest 200 △T	Smallest 200 △T
0-4	2229	57 △	7 ▼	1082	9 ▼	16 ▼	1209	29 NS	6 ▼	990	59 △	3 ▼
4-8	2226	40 NS	17 ▼	1074	4 ▼	15 ▼	1116	24 NS	6 ▼	1080	26 NS	11 ▼
8-12	2213	1 ▼	72 △	1048	0 ▼	101 △	1115	0 ▼	115 △	1080	1 ▼	95 △
12-16	2222	2 ▼	62 △	1067	20 ▼	34 NS	1116	6 ▼	61 △	1066	0 ▼	48 △
16-20	2225	26 NS	33 NS	1062	131 △	19 ▼	1116	101 △	6 ▼	1080	24 NS	27 NS
20-24	2231	74 △	9 ▼	1079	36 NS	15 ▼	1023	40 NS	6 ▼	1080	90 △	16 ▼

When compared with distribution of the total cases of validation data, △ greater at $p < 0.05$; ▼ smaller at $p < 0.05$; NS not significantly different from the pattern of the entire validation data

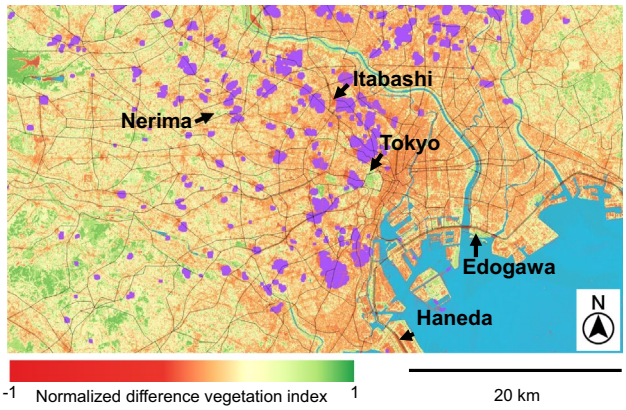

Fig. 8 Normalized difference vegetation index for the pixels representing 30 × 30 m areas around the meteorological stations at 10:15 AM on 6 August 2015. The arrows indicate the locations of the meteorological stations. The purple pixels indicate cloud and its shadow

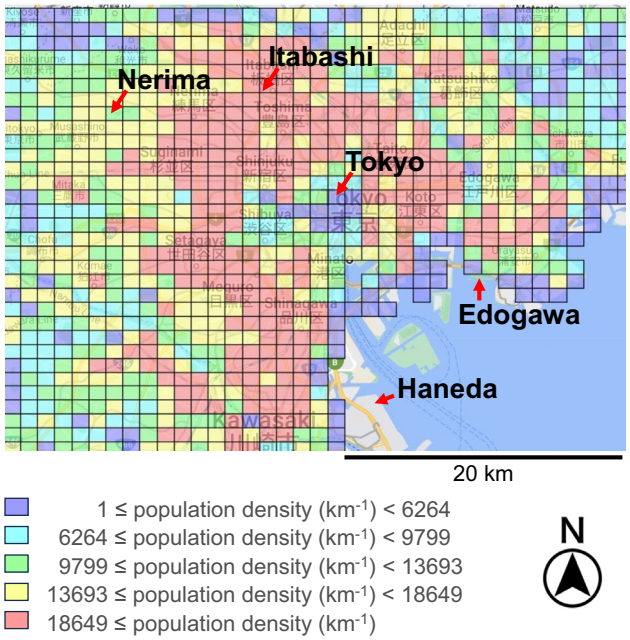

Fig. 9 Population density in Tokyo according to the 2020 census. The grids indicate 1 × 1 km squares. The red arrows indicate the locations of the meteorological stations

3.3 Additive Effects of Seaside Meteorological Data on $\Delta T_{ITB\text{-}TKY}$ Predictability

The author investigated if the addition of data from the seaside sites of Haneda and Edogawa improved the ΔT predictability. When the smallest 200 $\Delta T_{ITB\text{-}TKY}$ values were estimated for the August dataset, the Itabashi site was, to some extent, independent ($|R| < 0.37$; Table 5) from the other sites that had a common tendency of south–north wind speeds ($R > 0.70$).

Table 4 Time slots for the cases of the estimated smallest/greatest 200 $\Delta T_{Itabashi–Nerima}$ values

Time slot	August 2017-2022					January 2018-2020				
	Total cases	Greatest 200 △T		Smallest 200 △T		Total cases	Greatest 200 △T		Smallest 200 △T	
0-4	2232	66	△	0	▼	1116	52	△	9	▼
4-8	2232	44	NS	6	▼	1110	60	△	3	▼
8-12	2232	5	▼	53	△	1110	0	▼	107	△
12-16	2232	13	▼	105	△	1116	2	▼	73	△
16-20	2232	26	NS	35	NS	1116	28	NS	4	▼
20-24	2231	46	△	1	▼	1116	58	△	4	▼

When compared with distribution of the total cases of validation data, △ greater at $p < 0.05$; ▼ smaller at $p < 0.05$; NS not significantly different from the pattern of the entire validation data

The wind components from the Edogawa and Haneda sites had greater correlations with those at the Tokyo site. When Edogawa and Haneda data on temperature and wind speed/direction were involved, the R^2 value for $\Delta T_{ITB\text{-}TKY}$ improved to 0.71 from 0.55, suggesting the significant effects of wind from the seaside sites, as well as more unknown errors that accounted for 29% of the total variation of $\Delta T_{ITB\text{-}TKY}$.

When the smallest 200 $\Delta T_{ITB\text{-}TKY}$ values were estimated in August, the Haneda and Edogawa site had strong winds, mainly from the east and south (Fig. 10). West–east wind speed revealed different correlation patterns from those for south–north wind speed (Table 5). When the smallest 200 $\Delta T_{ITB\text{-}TKY}$ were estimated, the four sites had significant correlations with one another ($R > 0.65$). When the greatest 200 $\Delta T_{ITB\text{-}TKY}$ were estimated, the Itabashi and Tokyo sites had a significant correlation, whereas there was no correlation with the Haneda nor Edogawa sites. Meanwhile, the Haneda and Edogawa sites had a significant correlation in the west–east wind speed.

3.4 Land and Water Surface Temperatures Around the Nerima Site

At the Nerima site, 0.5 mm of precipitation was recorded on 13 July 2023. Since then, until the time of surface measurements on 27 July 2023, no precipitation was observed. The mean surface temperatures for the lawn space and the pond water near the Nerima site were 23.4 °C (±0.5 °C as standard deviation, N = 8) and 26.6 °C (±0.5 °C as standard deviation, N = 7), respectively. The air temperature was 26.2 °C at that time (4:10 AM).

4 Discussion

The above results indicated the generation of cool air plumes at the Tokyo and Nerima sites. Between the sites or the seasons, there seems to have been different conditions

Table 5 Correlation coefficients (R) between the meteorological stations in south–north or west–east wind speeds when the smallest/greatest 200 $\Delta T_{Itabashi\text{-}Tokyo}$ were estimated from the August 2017–2022 validation dataset

Site	Smallest 200 $\triangle T_{Itabashi\text{-}Tokyo}$				Greatest 200 $\triangle T_{Itabashi\text{-}Tokyo}$			
	Itabashi	Tokyo	Edogawa	Haneda	Itabashi	Tokyo	Edogawa	Haneda
Itabashi		0.78*	0.66*	0.66*		0.78*	0.09	0.08
Tokyo	**0.36***		0.76*	0.71*	**0.36***		0.11	0.08
Edogawa	**0.25***	**0.71***		0.88*	**-0.06**	**-0.04**		0.44*
Haneda	**0.33***	**0.73***	**0.91***		**-0.05**	**-0.05**	**0.84***	

* Significant correlation at $p < 0.05$

The black letters on a white background indicate correlation coefficients (R) for the west–east wind speed vector, while the white letters on a black background depict R values for the south–north wind speed vector

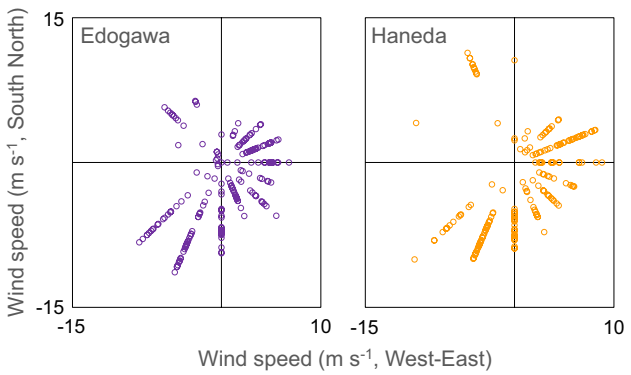

Fig. 10 Wind directions and speeds at the Edogawa and Haneda meteorological stations at the August time points of the smallest 200 $\Delta T_{Tokyo\text{-}Itabashi}$ values estimated by machine learning of the meteorological data from the Itabashi and Tokyo sites

and mechanisms for cool air plume generation and disappearance. The details will be discussed in the following sub-sections.

4.1 The Climatic Conditions of the Tokyo Region

In August, the entire Tokyo region is dominated by warm and humid southern winds, which results in more precipitation than in January (Table 1) when the prevailing dry winds come mainly from the northwesterly direction (Yoshino and Kazuko 1981). Within the 33 × 25 km area in Fig. 1, spatial variations in air temperature and wind occur. The differences in distance from the sea are known to contribute to the climatic differences, according to Saito (Saito 1976).

In Würzburg, Germany, even within a smaller area of approximately 3 × 5 km, the downtown area and a forest differed in air temperature by up to 8 °C in late July 2019 (Rahman et al. 2022). Lembrechts (2023) simulated that constructing high-story buildings after clearance of ordinary houses and trees significantly increased the air temperature of the area. The western side of the Nerima site is a residential area mainly consisting of ordinary houses, while the Itabashi site is surrounded by tall concrete buildings and negligible green areas (Figs. 1 and 8). These differences were obviously associated with temperature and wind differences (Table 1, Figs. 4 and 7).

4.2 Cool Air Plume and its Seepage

During some nights, the Tokyo site was shown to be covered by the cool air plume from the nearby trees and the adjacent Imperial Palace, while the Itabashi site was affected by heat sources in the highly populated areas around the city hall (Figs. 1 and 9). The cool trend at the Tokyo site after dark (Table 3) was previously reported by Narita et al. (2009), who measured precise changes in temperature, wind direction, and wind speed in the Imperial Palace and the surrounding urban areas. They observed that the cooling effect was pronounced when the site had calm wind, as shown in this study. A review article by Gunawardena et al. (2017) systematically explained the cooling effect in association with urban heat islands. Each tree and the leaves were cooled by releasing latent heat, as observed in the vertical thermal profiles of the tree canopy (Kato et al. 2015). Radiative cooling is a mechanism in which heat is lost from the ground and is known to cool the environment (Narita et al. 2002). These cooling mechanisms accumulate cool air in the green area (Sugawara et al. 2008), resulting in a cool air plume. Especially on nights with calm wind (< 5 m s^{-1}), the cooling system generates air circulation. Warmer air rises from the surrounding urban areas generating the low-altitude advection currents that draw cool air seepage from green areas (Oke 1989). This seeping generates a circulation system that completes its cycle with the subsidence of warmer urban air from above into the green area.

A required condition of this circulation's stability is the calm wind speed (< 5 m s^{-1}) because stronger wind impedes the vertical air movement and disrupts buoyancy-driven effects by introducing rapid turbulent mixing. These

processes of cool air seepage from the parks in Tokyo were further described more precisely in previous reports. For example, in Shinjuku Gyoen Park, another green area of Tokyo, Narita et al. (2004) observed precise spatiotemporal changes in air temperature in early August. The park and adjacent urban areas had the greatest ΔT values from late at night (22.00 PM) until the early morning (6.00 AM). Within 8 h, the wind speeds dropped from 3 m s^{-1} to less than 1.5 m s^{-1}. A similar negative correlation between wind speed and cooling effect has been observed in Davis, California, USA (Taha et al. 1989).

Rather than the cooling effects of tree canopies, the Nerima site in January uniquely suggested the occurrence of radiative cooling between late night and early morning (20.00 to 8.00) (Table 4) because of the open lawn (Fig. 1) and extremely calm wind (Fig. 7d) (Narita et al. 2002). These conditions are known to release heat more easily than tree canopies, especially when the sky is clear (Kawai and Kanda 2010) and the wind is calm (Sugawara et al. 2008), as seen in similar sites in the Tokyo region. In the dominance of radiative cooling, the cooling mechanism based on the transpiration of tree leaves and the accompanied loss of latent heat must be less significant in the Nerima site in January. Likewise, in the Tokyo site, where the greatest $\Delta T_{ITB\text{-}TKY}$ values were estimated, the effect of radiative cooling seemed to be more significant in January than in August. At the time points, the Tokyo site experienced calm wind from the adjacent western area with an open lawn space and dozens of large deciduous trees. From a scale-wise point of view, these cooling processes in the green areas were microscale (Young et al. 2005) and local-scale (Varentsov et al. 2021) processes that occurred within a distance of two to some hundred meters away from the edge of the green area.

4.3 Microscale, Local-Scale, and Mesoscale Effects in Association with Cooling and Heating the Sites

Contrary to the cool nights with the calm wind (Fig. 7a–d, Table 3), during the daytime, the Tokyo site tended to be subjected to warm air from the downtown area surrounding the green area. When the smallest 200 $\Delta T_{ITB\text{-}TKY}$ values were estimated in August, the Tokyo metrological station was subjected to strong winds from all directions (Fig. 7a), indicating that hot air plumes occasionally came from the heat sources to the Tokyo site, beyond the Imperial Palace (Jabbar et al. 2023).

At the same time, the Itabashi City Hall seemed to have a relatively cooler northern wind. In Shinjuku Gyoen and Hibiya Park, other urban green areas in Tokyo, thermographic profiling of tree canopies between 12:01 PM and 12:53 PM in August demonstrated that the cooling effect is pronounced especially by tall trees (Kato et al. 2015). At the Tokyo site, the meteorological station has distances of 10–20 m from the closest tree canopies (Fig. 1). In Melbourne, Australia, a sensor located in similar conditions indicated the cooling effect of tree canopies even during the daytime (Motazedian et al. 2020). Therefore, the Tokyo site could receive the cooling effects from the tree canopies during the daytime. However, as the Tokyo site and Imperial Palace are surrounded by busy offices and other buildings in the downtown, during the daytime, due to the urban heat island effect, the downtown and the Imperial Palace may have a strong updraft (Bentley et al. 2010).

Meanwhile, when the smallest 200 $\Delta T_{ITB\text{-}TKY}$ values were estimated in August, the seaside sites of Edogawa and Haneda were dominated by strong eastern and southern winds (Table 5, Fig. 10). Hence, it is very likely that urban heat between the Tokyo site and either Edogawa or Haneda reached the Tokyo site due to the strong winds, so that the cooling effects of the tree canopies were completely canceled by mixing the cool air with the absolutely greater amount of warm air (Norton et al. 2013; Cosgrove and Berkelhammer 2018).

Thus, the mechanisms that cause the greatest and smallest $\Delta T_{ITB\text{-}TKY}$ values were indicated to be different, as revealed in Moscow (Varentsov et al. 2021). The greatest 200 $\Delta T_{ITB\text{-}TKY}$ values were estimated when the microscale to local-scale cooling processes were effective at the Tokyo site. Conversely, the smallest 200 $\Delta T_{ITB\text{-}TKY}$ values were strongly associated with the mesoscale heat transfer mediated by strong winds from the heat sources. Microscale to local-sale climatic effects (Johansson et al. 2009) are given within a small range of up to some hundred meters, while mesoscale cooling and warming mechanisms by strong winds produce effects on sites two to some hundred km away (Young et al. 2005). In January, the strong winds, mainly from northwest of the Tokyo site, were indicated to have brought warm air from the Tokyo downtown area within business hours (Table 3), while the Itabashi site was likely to have been cooled by strong winds from the northwestern area that is less inhabited (Fig. 9) and therefore with less urban structures as heat sources (Fig. 8).

From this viewpoint of scale, the Nerima site is unique. Figure 7e indicates hard-to-recognize differences in wind direction and speed when the smallest/greatest 200 $\Delta T_{ITB\text{-}NRM}$ values were estimated based on the August dataset. Apparently, the extreme ΔT values were hardly associated with microclimatic effects. Rather, the extreme ΔT values resembled the results of mesoscale climatic differences between the Itabashi and the Nerima sites in August (Fig. 4).

4.4 Uniqueness of the Park in Nerima

The Nerima site was expected to show the effects of cool air plumes from the park that stretches on the eastern side

(Fig. 1). Under similar conditions in Nagoya, Japan, the cooling effect of a park was recognized up to 500 m away from the park (Hamada and Ohta 2010). Referring to this instance, the Nerima site is close enough to tree canopies that could cool the meteorological station (Norton et al. 2013). Park cooling intensity was positively correlated with park size in Italy (Bacci et al. 2003) and Mexico (Barradas 1991). A rectangle-shaped small park of approximately 2 hectares was microclimatically effective in Melbourne (Motazedian et al. 2020), where the climate is similar to that of Tokyo. The cooling effect reached a downtown corner 150 m away from the park. In the park that includes the Nerima site, the pond alone spans 3.2 hectares (Sakaguchi and Akasaka 2014); hence the park would be large enough to reveal microclimatic effects, but the cooling effect was apparently canceled by mesoscale effects in August. One possible explanation is that the pond water was too warm (26.6 ± 0.5 °C) until early morning (4:10 AM) to reveal the cooling effect on the Nerima meteorological station (Gunawardena et al. 2017). In addition to the warm pond in summer, the narrow and long shape of the park (Fig. 1) could be another reason why the cooling effect was not recognized in August (Chibuike et al. 2018).

4.5 Cooling Tokyo and Other Large Cities

It is clear that the current study area (Fig. 1) has too many heat sources and too small green areas for thermal comfort in summer. Tokyo has less than 4% (area/area) green areas, while some other cities such as London have more than 30% green areas (Uršič and Tamano 2019). Venhari et al. suggested that, mesoclimatically, parks with greater areas are required to cool the environment (Venhari et al. 2017). Monteiro et al. estimated that widespread cooling of a city may come from greenspaces of 3–5 ha, set 150 m apart (Monteiro et al. 2016), although blocks filling these conditions are rare. In London, a small area referred to as Roehampton is located between large green areas. Due to this fortunate location, Roehampton easily obtains thermal comfort (Gunawardena et al. 2017). These examples are suggested as cooling solutions in temperate climate zones. But most urban areas do not have this advantage.

In Tokyo, in the daytime, mesoscale heat transfer supersedes the cooling effects of green areas. In Tokyo, as in Gyeong-In, Korea (Lee et al. 2009), non-residential buildings are the most significant heat sources and account for more than one-half of the total heat emission, while heat emission from industrial sectors and cars is becoming less significant (Ministry of the Environment Japan 2012). Therefore, mitigation of the urban heat island effect must be accompanied by diminishing heat emission and/or absorption that causes subsequent heat emission from the heated urban structures.

Because urban structures have significant urban heat island effects, an effective countermeasure should be taking action against these structures. One example is the use of materials that stop the conversion of solar radiation into the thermal energy absorbed by urban structures (Doi 2022). One idea is to increase thermal comfort by constructing buildings along rivers at specific directions to effectively take the cool airflow generated by rivers (Narita 2006). Combining the greening of urban structures and various other countermeasures against the urban heat island effect should be favorable (Irie 2022; Giridharan and Emmanuel 2018).

Such combinations of countermeasures to mitigate urban heat island effects are expected to function in cities in other climatic zones than temperate zones in addition to those in temperate zones. Jeddah, Saudi Arabia, is located in an arid climatic zone. The climate is categorized as a hot desert climate, in which water availability is much lower, while the summer lasts longer than in Tokyo. The annual precipitation is 60 mm, but this amount is estimated to be adequate to enable urban green infrastructures if the large amounts of precipitation that currently remain lost are kept under control (Bogis et al. 2021). In Saudi Arabia, fortunately, rooftop and vertical wall greening is well supported by local communities (Maghrabi et al. 2021). In Dhahran, another city in Saudi Arabia, a greening strategy reduced electricity consumption for air conditioning by approximately 35% (Mahmoud et al. 2017). In Johor Bahru, Malaysia, under its tropical rainforest climate, the greening of rooftops reduced the temperature in the rooms below by more than 4 °C (Rashid and Ahmed 2009). This cooling effect is marked because an increase in global air temperature of 1.5 °C results in a 37% increment in heat-related deaths (Vicedo-Cabrera et al. 2021). Rooftop greening and other greening methods have high feasibility, and are thus worth considering in regions in tropical and hot arid climatic zones, in addition to temperate zones. These effects in the above regions are worth investigating in terms of thermal comfort, mortality, and energy consumption, mainly due to air conditioning. Expanding these viewpoints, urban greening components have been depicted by Khan and Li (2024).

In some cities and countries including Tokyo, the declining population may help the mitigation by decreasing the demand for real estate properties (Uto et al. 2023), followed by constructing new green areas. More fundamentally, human population control should be added as the 18th or 0th sustainable development goal because it is the most fundamental cause of the urban heat island phenomenon, global warming, and other challenges to sustainable socioeconomic development.

4.6 Technical Aspects, Limitations of this Study, and Prospective

The values of the slope (< 0.755) for the regression in Fig. 6 show that the effectiveness of the independent variables on ΔT estimation was limited (Choudhry et al. 2012). Some possible causes may be enlisted. Among the sites, occasionally, differences in precipitation within 10 min occurred. In the comparison between the Itabashi and Nerima sites in August, among the 26,783 cases, there were 889 cases in which precipitation differences (0 <|difference|) were recognized. According to Table 2, year was a significant source of the total variation of ΔT (Table 2), though this was not expected. In addition to the natural differences, anthropogenic factors such as changes in the intensity of heat sources at different time points and on days are likely to have contributed, as in Paris, where the intensity of heat sources was 20% smaller on Sundays than weekdays (de Munck et al. 2013).

ΔT is not described by the intensity of the cooling effects of green areas alone. The intensity of the mesoscale heat transfer is another determinant of ΔT. The improvement in $\Delta T_{ITB\text{-}TKY}$ predictability from an R^2 value of 0.55 to 0.71 by including the Edogawa and Haneda data demonstrates the significance of various unknown heat sources between the Tokyo site and the seaside sites more than 10 km apart from the Tokyo site. More unknown sources account for 29% of the total variation. Therefore, these multiple cooling/heating variables that do not necessarily have correlations with one another make accurate ΔT estimation difficult. At the same time, therefore, combining data from other sites than those to be compared will be helpful because urban morphological and land use patterns are complex (Figs. 8, 9, 10, Table 5). Adding wind and other meteorological data from more stations will make the ΔT value more predictable because these data are likely to have an association with ΔT. Alternatively, as de Munck et al. (2013) suggested, socioeconomic and other variables such as traffic data (Husni et al. 2022) may be incorporated into the calculation to determine its relative significance compared with meteorological variables.

Also, the current approach does not elucidate precise changes in canopies, forests, and parks, including vertical changes in temperature and wind. Hence, combining the current approach and the techniques of precise measurements and analysis applied by the authors in previous studies [e.g., (Kato et al. 2015; Narita et al. 2004)] would reveal more facts about the cooling effects of urban green areas. Previous studies with precise measurements have been conducted within periods of up to a week. These period could be extended because, at this time, various sensors and loggers are becoming widely available at a reasonable cost. Some loggers have large enough capacities to record temperature and other meteorological records for multiple years at a time resolution of 10 min, and are thus applicable to long-term studies on forest canopy microclimates (Von Arx et al. 2012). These tools and the current approach employing artificial intelligence will visualize more precise behavioral patterns of cool air plumes in green areas. These precise observations may generate three-dimensional plots or videos that show the size, shape, boundary between, and movement of cool and hot/warm air plumes.

5 Conclusions

This is the first study to visualize cool air plumes from urban green areas using wind directions and speeds at meteorological stations in green areas and compare their air temperatures with those at an urban site by relying on artificial intelligence. ΔT values for multiple years were determined, resulting in more than 12,800 cases incorporated into the neuro-evolution of an artificial intelligence architecture. The analyses of wind directions and speeds for the cases of extremely small and large ΔT values revealed cooling effects as the result of microscale and local-scale climatic processes in the green areas. The occurrence of cool air plumes was recognized during nights with calm winds in green areas, indicating the effects of the loss of latent heat from the canopies and/or radiative cooling of unpaved open areas.

Meanwhile, the other extreme ΔT values showed that the green areas became hotter/warmer than the urban site. In these cases, the green areas were indicated to be subjected to strong hot/warm winds from the urban heat sources surrounding/near the green areas. Hence, the heat transfer to the green areas was thought to be a mesoscale climatic process.

This current approach is valuable and worth extending to other cities in subtropical, tropical, and hot arid regions. The current approach involved a large number of cases, more than 12,800 over multiple years. Artificial intelligence will be valuable because the number of cases and the period of time enhance the statistical reliability of predicting the cool air plume appearance, as well as its disappearance. The advantage will be pronounced, especially if the current approach is combined with precise in situ measurements such as three-dimensional profiling of canopy and air temperature in and around urban green areas, especially if the precise measurements were automated. This combination should bridge the mid- to long-term analysis of cool air plume behavior and the precise understanding of in situ processes. Hence, this combination is expected to contribute to the mitigation of the urban heat island effect by providing basic information on cool air plumes from urban green areas. The reliable information based on precise and long-term observations of cool air plumes and the generation processes will aid in urban planning to enable the mitigation

of the urban heat island phenomenon by relying on urban green areas.

Funding The author received no financial support for the research, authorship, and/or publication of this article.

Declarations

Conflict of interest The author declares no conflict of interest regarding this article.

References

Afrin S, Islam MM, Ahmed T (2021) A meteorology based particulate matter prediction model for megacity Dhaka. Aerosol Air Qual Res 21:200371. https://doi.org/10.4209/aaqr.2020.07.0371

Akihito ST, Teduka M, Kawada S (2016) Long-term trends in food habits of the raccoon dog, *Nyctereutes viverrinus*, in the Imperial palace, Tokyo. Bull Natl Mus Nat Sci Ser A 42:143–161

Altan H, Alshikh Z, Belpoliti V et al (2019) An experimental study of the impact of cool roof on solar PV electricity generations on building rooftops in Sharjah, UAE. Int J Low-Carbon Technol 14:267–276. https://doi.org/10.1093/ijlct/ctz008

Bacci L, Morabito M, Raschi A, Ugolini F (2003) Thermohygrometric conditions of some urban parks of Florence (Italy) and their effects on human well-being. Trees 6:49

Barradas VL (1991) Air temperature and humidity and human comfort index of some city parks of Mexico City. Int J Biometeorol 35:24–28. https://doi.org/10.1007/BF01040959

Bentley M, Stallins T, Ashley W (2010) The Atlanta thunderstorm effect. Weatherwise 63:24–29. https://doi.org/10.1080/00431671003609937

Bogis A, Bork D, Miller P (2021) Are green infrastructure strategies suitable in arid climates? A design feasibility study from Jeddah City, Saudi Arabia. Int J Archit Plan 1:9–18. https://doi.org/10.51483/ijarp.1.1.2021.9-18

Chibuike EM, Ibukun AO, Abbas A, Kunda JJ (2018) Assessment of green parks cooling effect on Abuja urban microclimate using geospatial techniques. Remote Sens Appl: Soc Environ 11:11–21. https://doi.org/10.1016/j.rsase.2018.04.006

Choudhry P, Misra A, Tripathi S (2012) Study of MODIS derived AOD at three different locations in the Indo Gangetic Plain: Kanpur. Gandhi College and Nainital. Copernicus Publications, Göttingen, pp 1479–1493. https://doi.org/10.5194/angeo-30-1479-2012

Cosgrove A, Berkelhammer M (2018) Downwind footprint of an urban heat island on air and lake temperatures. Npj Clim Atmos Sci 1:46. https://doi.org/10.1038/s41612-018-0055-3

de Munck C, Pigeon G, Masson V et al (2013) How much can air conditioning increase air temperatures for a city like Paris, France? Int J Climatol 33:210–227. https://doi.org/10.1002/joc.3415

Doi R (2019) Maximizing the accuracy of continuous quantification measures using discrete packtest products with deep learning and pseudocolor imaging. J Anal Methods Chem 2019:1685382. https://doi.org/10.1155/2019/1685382

Doi R (2021) Assessing the reforestation effects of plantation plots in the Thai savanna based on 45 cm resolution true-color images and machine learning. Environ Res Lett 16:014030. https://doi.org/10.1088/1748-9326/abcfe3

Doi R (2022) Are new residential areas cooler than older ones? Emerg Sci J 6:1346–1357. https://doi.org/10.28991/ESJ-2022-06-06-08

Farkas JZ, Hoyk E, de Morais MB, Csomós G (2023) A systematic review of urban green space research over the last 30 years: a bibliometric analysis. Heliyon. https://doi.org/10.1016/j.heliyon.2023.e13406

Giridharan R, Emmanuel R (2018) The impact of urban compactness, comfort strategies and energy consumption on tropical urban heat island intensity: a review. Sustain Cities Soc 40:677–687. https://doi.org/10.1016/j.scs.2018.01.024

Gunawardena K, Wells M, Kershaw T (2017) Utilising green and bluespace to mitigate urban heat island intensity. Sci Total Environ 584:1040–1055. https://doi.org/10.1016/j.scitotenv.2017.01.158

Hamada S, Ohta T (2010) Seasonal variations in the cooling effect of urban green areas on surrounding urban areas. Urban for Urban Green 9:15–24. https://doi.org/10.1016/j.ufug.2009.10.002

Husni E, Prayoga GA, Tamba JD et al (2022) Microclimate investigation of vehicular traffic on the urban heat island through IoT-based device. Heliyon. https://doi.org/10.1016/j.heliyon.2022.e11739

Irie T (2022) The cooling effect of green infrastructure in mitigating nocturnal urban heat islands: a case study of Yoyogi Park and Meiji Jingu Shrine in Tokyo. Landsc Res 47:559–583. https://doi.org/10.1080/01426397.2022.2050195

Jabbar HK, Hamoodi MN, Al-Hameedawi AN (2023) Urban heat islands: a review of contributing factors, effects and data. IOP Publ 1129:012038. https://doi.org/10.1088/1755-1315/1129/1/012038

Johansson E, Ouahrani D, Shaker Al-Asir H et al (2009) Climate conscious architecture and urban design in Jordan-towards energy efficient buildings and improved urban microclimate. Report 12

Kato T, Tebakari T, Yamada T, Hino M (2006) Vertical and horizontal structure of air temperature and humidity in urban park forest and its surrounding. Proc Hydraul Eng 50:505–510. https://doi.org/10.2208/prohe.50.505

Kato A, Okitsu Y, Tsunematsu N et al (2015) Mitigation effect of urban heat island from forest canopy structure of urban forest. J Jpn Soc Reveget Technol 41:169–174. https://doi.org/10.7211/jjsrt.41.169

Kawai T, Kanda M (2010) Urban energy balance obtained from the comprehensive outdoor scale model experiment. Part I: basic features of the surface energy balance. J Appl Meteorol Climatol 49:1341–1359. https://doi.org/10.1175/2010JAMC1993.1

Khan MS, Li Y (2024) Comparative study and effects of urban green scape on the land surface temperature of a large metropolis and green city. Heliyon. https://doi.org/10.1016/j.heliyon.2024.e24912

Köppen WP (1931) Grundriss der klimakunde. Walter de Gruyter

Lee S-H, Song C-K, Baik J-J, Park S-U (2009) Estimation of anthropogenic heat emission in the Gyeong-In region of Korea. Theoret Appl Climatol 96:291–303. https://doi.org/10.1007/s00704-008-0040-6

Lembrechts JJ (2023) Microclimate alters the picture. Nat Clim Change 13:1–2. https://doi.org/10.1038/s41558-023-01632-5

Maghrabi A, Alyamani A, Addas A (2021) Exploring pattern of green spaces (Gss) and their impact on climatic change mitigation and adaptation strategies: evidence from a Saudi Arabian city. Forests 12:629. https://doi.org/10.3390/f12050629

Mahmoud AS, Asif M, Hassanain MA et al (2017) Energy and economic evaluation of green roofs for residential buildings in hot-humid climates. Buildings 7:30. https://doi.org/10.3390/buildings7020030

Mei S-J, Yuan C (2022) Urban buoyancy-driven air flow and modelling method: a critical review. Build Environ 210:108708. https://doi.org/10.1016/j.buildenv.2021.108708

Ministry of the Environment, Japan (2012) Manual of countermeasures for heat island

Monteiro MV, Doick KJ, Handley P, Peace A (2016) The impact of greenspace size on the extent of local nocturnal air temperature cooling in London. Urban for Urban Green 16:160–169. https://doi.org/10.1016/j.ufug.2016.02.008

Moschella M, Tucci M, Crisostomi E, Betti A (2019) A machine learning model for long-term power generation forecasting at bidding zone level. IEEE, pp 1–5. https://doi.org/10.48550/arXiv.1910.03276

Motazedian A, Coutts AM, Tapper NJ (2020) The microclimatic interaction of a small urban park in central Melbourne with its surrounding urban environment during heat events. Urban for Urban Green 52:126688. https://doi.org/10.1016/j.ufug.2020.126688

Narita K-I (2006) Ventilation path and urban climate. Wind Eng JAWE 2006:109–114. https://doi.org/10.5359/jawe.2006.109

Narita K, Mikami T, Sugawara H et al (2004) Cool-island and cold air-seeping phenomena in an urban park, Shinjuku Gyoen, Tokyo. Geogr Rev Japan 77:403–420. https://doi.org/10.4157/grj.77.403

Narita K, Mikami T, Honjo T et al (2002) 8.2 Observations about cool-island phenomena in urban park

Narita K, Sugawara H, Yokoyama H, et al (2009) Cold air seeping from an urban green space, imperial palace, in central Tokyo

Norton B, Bosomworth K, Coutts A et al (2013) Planning for a cooler future: green infrastructure to reduce urban heat. Victorian Centre for Climate Change Adaptation Research. https://doi.org/10.13140/2.1.2430.1764

O'Malley C, Kikumoto H (2021) An investigation into the relationship between remotely sensed land surface temperatures and heat stroke incident rates in the Tokyo Prefecture 2010–2019. Sustain Cities Soc 71:102988. https://doi.org/10.1016/j.scs.2021.102988

Oke TR (1989) The micrometeorology of the urban forest. Philos Trans R Soc Lond B, Biol Sci 324:335–349. https://doi.org/10.1098/rstb.1989.0051

Oukawa GY, Krecl P, Targino AC (2022) Fine-scale modeling of the urban heat island: a comparison of multiple linear regression and random forest approaches. Sci Total Environ 815:152836. https://doi.org/10.1016/j.scitotenv.2021.152836

Pichler M, Hartig F (2023) Machine learning and deep learning—a review for ecologists. Methods Ecol Evol 14:994–1016. https://doi.org/10.1111/2041-210X.14061

Rahman MA, Franceschi E, Pattnaik N et al (2022) Spatial and temporal changes of outdoor thermal stress: influence of urban land cover types. Sci Rep 12:671. https://doi.org/10.1038/s41598-021-04669-8

Rashid R, Ahmed MHB (2009) Thermal performance of rooftop greenery system at the tropical climate of Malaysia a case study of a 10 storied building RCC flat rooftop at UTM, Johor Bahru, Malaysia. Dimensi J Archit Built Environ 37:41–50. https://doi.org/10.9744/dimensi.37.1.pp.%2041-50

Rizwan AM, Dennis LY, Chunho L (2008) A review on the generation, determination and mitigation of Urban Heat Island. J Environ Sci 20:120–128. https://doi.org/10.1016/s1001-0742(08)60019-4

Rouse J, Haas R, Schell J, Deering D (1974) Monitoring vegetation systems in the Great Plains with ERTS. NASA Spec Publ 351:309

Saito N (1976) Numerical experiments of the land and sea breeze circulation. Pap Meteorol Geophys 27:99–117. https://doi.org/10.2467/mripapers1950.27.4_99

Sakaguchi M, Akasaka I (2014) Cool-island phenomena and Cold-air Seeping-out effect in Shakujii Park. In: Proc. annual meeting of the Association of Japanese Geographers, Autumn 2014, p 101. https://doi.org/10.14866/ajg.2014a.0_101

Skubalska-Rafajłowicz E (2014) Small sample size in high dimensional space-minimum distance based classification. In: Artificial intelligence and soft computing (ICAISC 2014). Springer, pp 610–621

Stewart ID, Mills G (2021) The urban heat island. Elsevier

Sugawara H, Tanaka H, Narita K et al (2008) How much cool air does an urban green park produce. Geogr Rep Tokyo Metrop Univ 43:83–89

Sugawara H, Narita K, Mikami T (2021) Vertical structure of the cool island in a large urban park. Urban Clim 35:100744. https://doi.org/10.1016/j.uclim.2020.100744

Taha H, Akbari H, Rosenfeld A (1989) Vegetation canopy micro-climate: a field-project in Davis, California

Tzavali A, Paravantis JP, Mihalakakou G et al (2015) Urban heat island intensity: a literature review. Fresenius Environ Bull 24:4537–4554

Uršič M, Tamano K (2019) The importance of green amenities for small creative actors in Tokyo: comparing natural and sociocultural spatial attraction characteristics. Acta Geogr Slov 59:159–172. https://doi.org/10.3986/AGS.4710

Uto M, Nakagawa M, Buhnik S (2023) Effects of housing asset deflation on shrinking cities: a case of the Tokyo metropolitan area. Cities 132:104062. https://doi.org/10.1016/j.cities.2022.104062

Varentsov M, Fenner D, Meier F et al (2021) Quantifying local and mesoscale drivers of the urban heat island of Moscow with reference and crowdsourced observations. Front Environ Sci 9:543. https://doi.org/10.3389/fenvs.2021.716968

Venhari AA, Tenpierik M, Hakak AM (2017) Heat mitigation by greening the cities, a review study. Environ Earth Ecol 1:5–32. https://doi.org/10.24051/eee/67281

Vicedo-Cabrera AM, Scovronick N, Sera F et al (2021) The burden of heat-related mortality attributable to recent human-induced climate change. Nat Clim Change 11:492–500. https://doi.org/10.1038/s41558-021-01058-x

Von Arx G, Dobbertin M, Rebetez M (2012) Spatio-temporal effects of forest canopy on understory microclimate in a long-term experiment in Switzerland. Agric for Meteorol 166:144–155. https://doi.org/10.1016/j.agrformet.2012.07.018

Yaşlı R, Yücedağ C, Ayan S, Simovski B (2023) The role of urban trees in reducing land surface temperature. SilvaWorld 2:36–49. https://doi.org/10.29329/silva.2023.518.05

Yoshino MM, Kazuko U (1981) Regionality of climatic change in East Asia. GeoJournal 5:123–132. https://doi.org/10.1007/BF02582045

Young GS, Sikora T, Winstead N (2005) Use of synthetic aperture radar in finescale surface analysis of synoptic-scale fronts at sea. Weather Forecast 20:311–327. https://doi.org/10.1175/WAF853.1